SANDIA REPORT
SAND2001-1338
Unlimited Release
Printed November 2001

Numerical Simulation of the Partial Catalytic Oxidation of Ethane to Ethylene in Short Contact Time Reactors

R. P. Pawlowski and A. G. Salinger

Prepared by
Sandia National Laboratories
Albuquerque, New Mexico 87185 and Livermore, California 94550

Sandia is a multiprogram laboratory operated by Sandia Corporation, a Lockheed Martin Company, for the United States Department of Energy under Contract DE-AC04-94AL85000.

Issued by Sandia National Laboratories, operated for the United States Department of Energy by Sandia Corporation.

Available to DOE and DOE contractors from
U.S. Department of Energy
Office of Scientific and Technical Information
P.O. Box 62
Oak Ridge, TN 37831

Telephone: (865)576-8401
Facsimile: (865)576-5728
E-Mail: reports@adonis.osti.gov
Online ordering: http://www.doe.gov/bridge

Available to the public from
U.S. Department of Commerce
National Technical Information Service
5285 Port Royal Rd
Springfield, VA 22161

Telephone: (800)553-6847
Facsimile: (703)605-6900
E-Mail: orders@ntis.fedworld.gov
Online order: http://www.ntis.gov/ordering.htm

Numerical Simulation of the Partial Catalytic Oxidation of Ethane to Ethylene in Short Contact Time Reactors

R.P. Pawlowski and A.G. Salinger

Sandia National Laboratories, Albuquerque, NM 87185

Abstract

The partial catalytic oxidation of ethane to ethylene in short contact time reactors is studied numerically. A single channel of a platinum-coated monolith reactor is modeled, including fully coupled fluid mechanics, heat transfer, and multicomponent species transport. The model includes a detailed chemistry mechanism of Zerkle and Allendorf that involves 22 gas phase species involved in 77 reversible reactions, and 14 surface species and 35 surface reactions on the platinum surfaces. The model also includes conjugate heat transfer in the reactor wall. This highly coupled and nonlinear system was solved using the MPSalsa parallel reacting flows code. The fully-coupled Newton method employed in MPSalsa allowed for rapid analysis steady-state solution branches. Several parameter studies were performed on this model to investigate the effect of key parameters on system performance, as measured by selectivity and conversion results.

1 Introduction

Ethylene is one of the most widely used chemicals, with the US producing 25 billion kilograms annually. The current production technique is steam cracking in which alkanes must be heated to high temperatures (~800 K). To

produce the energy required for steam cracking, undesired products are fed into the furnace to be burned. Although energy efficient, the process converts >10% of the ethane into CO_2 [1]. Due to the high flame temperatures, pollutants such as NO_x are also produced. Recently, a different process, catalytic partial oxidation (CPO) over a metal surface, has been suggested to replace steam cracking. The CPO of ethane to ethylene is exothermic, generating enough energy to run the process autothermally. Additionally, the residence time is several orders of magnitude lower than steam cracking. This process has the potential to revolutionize the industrial production of one of the most produced chemicals in the world by increasing ethylene production rates by several orders of magnitude, simplifying process equipment by eliminating the need for external heating, and reducing pollution emissions.

The standard production process of steam cracking produces ∼85% selectivity with a conversion of ∼60% of ethane. Using Pt-coated foam monoliths, Huff and Schmidt [2, 3] found that a selectivity of ∼65% to ethylene could be achieved at a conversion of ∼70%. Adding Sn to the Pt surface increased the selectivity to ∼70%. Recently, it was found that adding hydrogen as a radical scavenger could increase selectivity to >85% [1, 4] on the Pt-Sn catalytic surface, making it competitive with steam cracking.

The study of partial oxidation processes is generating great amounts interest because of the many advantages which can be gained through different synthesis routes. CPO is promising for the development of more selective processes which reduce unwanted by-products and use different and cheaper feedstocks in faster processes with lower capital costs [5]. CPO processes have demonstrated the ability to achieve high selectivities and high conversion with much faster residence times. The high energy release in such systems can result in autothermal operation, eliminating the need for an exterior heat source. These systems thus become much less complex and are usually much smaller in terms of process equipment (typically an order of magnitude smaller) than alternative process techniques. The difficulty of the process lies in that the standard catalytic analysis techniques fail for CPO processes. The oxidation process is two to three orders of magnitude faster which make kinetic measurements difficult because the reactions become mass transfer limited. Oxidation reactions are highly exothermic which lead to non-uniform temperature distributions throughout the catalyst and reactor. Finally, since the chemistry is autothermal, the potential for run-

away that can destroy the catalyst is a possibility. Homogeneous reaction can contribute to flames and explosions within the reactor. These factors preclude scale up from micro reactors (used to study kinetics) through bench scale, pilot plant and full scale plants. One must design the reaction system and reactor at the same time, running under actual full scale process conditions in temperature, pressure, and composition [5]. Schmidt and coworkers point out that "The standard paradigm of experimentalists and modelers doing separate research simply will not work because neither alone can deal with the critical issues in oxidation processes".

Another challenge in CPO is that porous pellets, the mainstay of heterogeneous catalysis, are poor performers in oxidation processes. They were developed for slow processes where maximum surface area is essential. In oxidation processes, where mass transfer limitations apply, only the external surface is used, wasting metal coatings on the inside of the pellets. This requires new designs in which geometry plays a critical factor in overall performance. Again, reactor design and reaction kinetics are demonstrated to be highly coupled and must be considered together. The emerging reactor of choice has become the monolith reactor. A monolith reactor consists of a series of densely packed channels. The channels can be straight, constructed from a tightly packed bundle of small diameter tubes or constructed from a porous solid, with highly tortuous channels as in the case of foam monoliths. Monoliths are typically constructed from wire gauze or ceramics such as α-alumina foams. Small sections of the tubes are coated with the noble metal catalyst, typically Pt, Sn, or Rh or in combination with each other.

CPO has been used in the past for many different processes. Nitric acid production utilizes the Ostwald process to oxidize ammonia to NO [6, 7]. The Andrussow process is used to produce HCN by ammoxidation of methane [7]. CPO reactors have been demonstrated to be highly effective in neutralizing volatile organic compounds (exhaust from paint booths, curing ovens, and the drying of inks and pulp products) and hazardous pollution emissions [8]. In the case of volatile organic compounds, conversion of 99.5% was achieved for contact times ranging from 4 to 12 ms (about 250 times faster than conventional techniques). CPO has shown great promise for the conversion of methane to syngas over Pt and Rh surfaces [9, 10, 11, 12, 13]. Methane is hazardous to transport and is typically converted to an intermediate for transport and to increase utilization [10]. Standard synthesis routes

include converting methane to methanol over Cu/ZnO catalysts and converting methane to hydrocarbon chains through a Fischer-Tropsch process over Fe and Ru catalysts. The residence times of such reactors are on the order of 1 s. Partial oxidation reactors can reduce this residence time to 10^{-3} s while reducing the size and complexity of the equipment involved.

The following work is based on a collaboration with DOW Chemical Company, the National Labs (Sandia and Los Alamos) and the University of Minnesota through the Office of Industrial Technology (OIT). While partners in the collaboration are studying the chemistry mechanisms both experimentally and computationally, the goal of this research was to take the existing proposed mechanisms and study how reactor design and operating conditions could influence selectivities and conversion. The idea was to search for parameters that could help lead to a greater understanding of the reaction-transport phenomena involved in partial oxidation and to look for regimes which could yield better production characteristics that have not been explored previously.

2 Model

The reactor under consideration is a straight tube monolith (a bundle of straight tube channels with the same inlet feed). The domain is constructed by modeling *one* of the straight tube channels with the assumption of axial symmetry, reducing the calculation to 2 dimensions in cylindrical coordinates. The reactor consisted of a 4 cm long tube. At the inlet is a 1 cm non-catalytic section (radiation shield), followed by a 1 cm section where the tube wall is bounded by a Pt coating, which is then followed by a 2 cm non-catalytic outlet section. The inside diameter of the tube is 0.6 mm. Since the tube is situated in the middle of a large bundle of similar tubes all generating enough heat to run autothermally, the outer tube wall can be considered adiabatic. Heat transfer in the tube wall is modeled to capture the influence of the thermal conduction on the temperature profile in the reactor. The tube wall thickness is 0.1 mm. The wall is assumed to be cold at the inlet and adiabatic on the outside wall, and has a thermal conductivity of 105 erg/(sec cm K). The inlet velocity and temperature are uniform.

The inlet species consist of ethane, oxygen, nitrogen and, in some cases, hydrogen. In all cases studied, a 0.3 mole fraction of N_2 is included in the inlet. The ethane and oxygen mole fractions were fixed based upon the specific carbon to oxygen ratio (C_2H_6/O_2) desired. Hydrogen was added to the feed as a radical scavenger in one of the parametric studies. In this case, the mole fractions were adjusted to include a fixed H_2/O_2 ratio. When inlet mole fractions are calculated, they are evaluated in terms of a carbon to oxygen ratio and a hydrogen to oxygen ratio, and always include a 0.3 mole fraction of nitrogen.

A set of controllable parameters and their standard conditions were defined as a starting point for this study. They consisted of the inlet velocity, V_{inlet}, set to 150 cm/s, the inlet temperature, T_{inlet}, at 300 K, the reactor pressure, P, at 1.4 atm, the carbon to oxygen ratio, C/O, at 1.8 and the hydrogen to oxygen ratio, H/O, at zero.

The reaction mechanism was supplied by Dave Zerkle of Los Alamos National Labs and comes from his collaboration with Mark Allendorf of Sandia National Labs. The mechanism consists of 22 gas-phase species with 77 reversible gas-phase reactions, and 17 surface species undergoing 35 surface reactions. The mechanism is listed in Appendix 4. The CHEMKIN and SURFACE CHEMKIN packages are used to provide rigorous treatment of the multicomponent transport properties and species production/consumption rates. All physical properties in the gas-phase are treated as functions of the local temperature and mole fractions and a global operating pressure. Through reaction source terms on the catalytic surface and in the gas-phase, autothermal operation of the reactor was realized.

Solutions to the governing set of 26 coupled PDEs were obtained using the Finite Element code MPSalsa developed by Sandia National Laboratories. The calculations presented here were on a fine mesh of 2727 nodes corresponding to 70902 unknowns. A fully coupled Newton method is used to solve for the unknowns. Currently, 5% of the solution time is spent forming the finite element equations and Jacobian matrix, and 95% in the linear solver. The Aztec linear solver package is used, and an ILUT preconditioner with overlap and fill-in and the GMRES iterative solver were selected. A slow time integration process was needed once to get to a first steady state solution. Once a steady state solution was achieved, all other solutions were

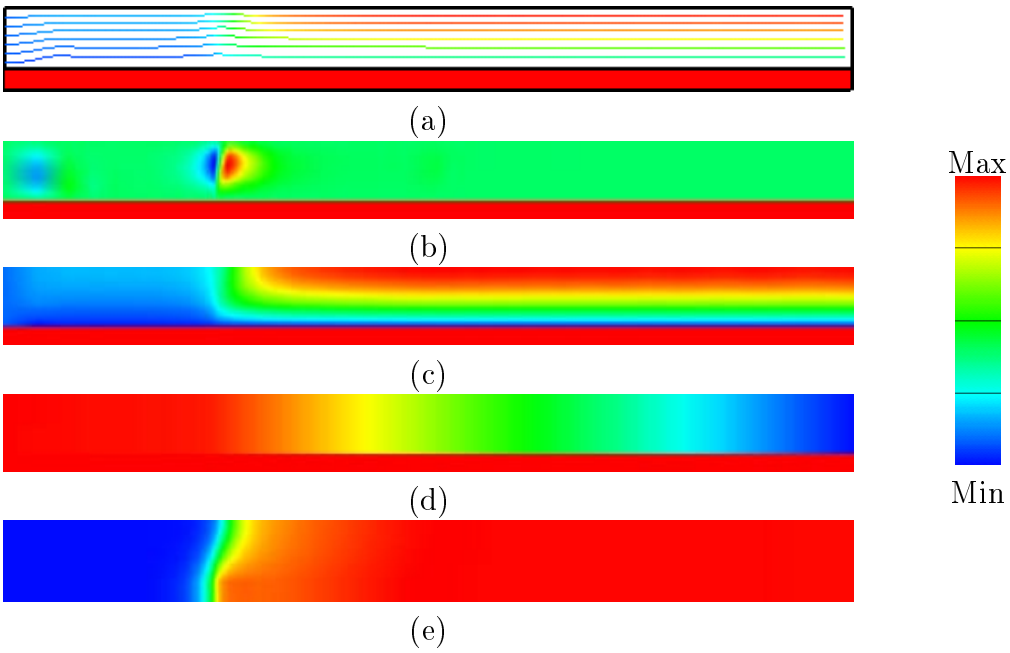

Figure 1: Solution profile at the standard conditions. V_{inlet}=150 cm/s, P=1.4 atm, T_{inlet}=300 K. (a) streamlines, (b) axial velocity, (c) radial velocity, (d) pressure, and (e) temperature.

calculated by steady state parameter continuation using the LOCA library developed by Andrew Salinger of Sandia National Laboratories.

Figure 1 represents the solution for the streamlines, velocities, pressure, and temperature through out the reactor at the standard conditions. For visualization purposes, the radial (vertical) dimension on the the plots has been stretched a factor of 10. The flow enters through the left side and exits through the right side. The IR and OR of the tube are 0.03 and 0.04 cm respectively. The top of the domain is the centerline of the tube (axis of symmetry) and the bottom is the tube wall (0.01 cm thick). The red blocks on the bottom of the domain represent the solid tube wall, where temperature is the only solution variable calculated. The solutions plotted are for a total domain length of 4.0 cm. The first 1 cm is the radiation shield that runs from the inlet to the beginning of the catalyst coating. The next 1 cm length has a Pt coating on the tube wall, and the final 2 cm is an outlet with no coating

Parameter	Standard Condition	Range	Units
Inlet Velocity	150	10-400	cm/s
Inlet Temperature	300	250-600	Kelvin
Pressure	1.4	0.5-10.0	atm
C/O Inlet Ratio	1.8	1.8-2.4	
H_2/O_2 Inlet Ratio	0.0	0.0-2.3	
Tube Radius	0.03	0.025-0.08	cm
Inlet N_2 Mole Fraction	0.3	0.3	

Table 1: Range of conditions used in the parametric study.

on the tube wall. The mesh was extended 2 cm past the catalytic section, where it appears that most reactions have reached equilibrium. Anything less than 2 cm was found to have appreciable gas-phase reaction taking place near the domain exit, indicating reaction equilibrium had not been reached.

Figure 2 depicts selected species mass fractions throughout the reactor at the standard conditions. Each species uses the same color scale at the right, but are scaled to their individual minimum and maximum mass fractions which are listed next to the species name.

The most interesting plot is the CO_2 mass fraction (Figure 2), that shows a very sharp peak right at the beginning of the catalyst. Design alternatives that restrict the oxygen concentration at this point may significantly decrease the selectivity to CO_2.

3 Parametric Study

A parametric study was undertaken to identify the optimal operating conditions and geometry at which to build and operate an experimental reactor based upon the currently proposed chemistry mechanisms. Table 1 lists the parameters studied and the ranges over which they were varied in the parametric study.

The first variable of interest was the inlet velocity. The velocity ranged from 10 to 400 cm/s. Figure 3 depicts the (a) conversion, (b) carbon selectivity,

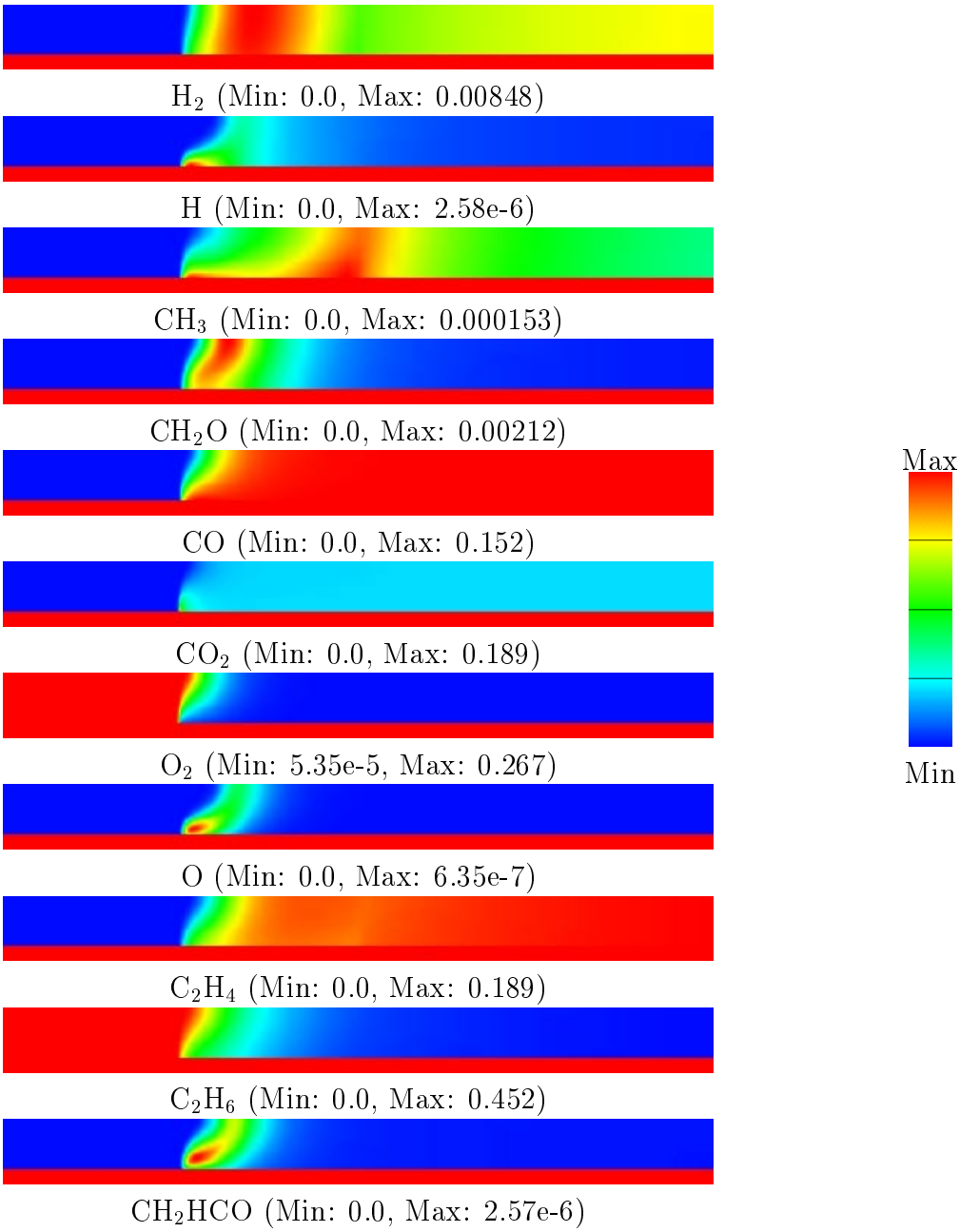

Figure 2: Mass Fractions of selected species at the standard conditions. V_{inlet}=150 cm/s, P=1.4 atm, C/O=1.8, and T_{inlet}=300 K.

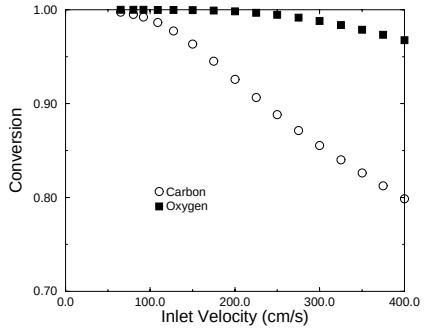

(a)

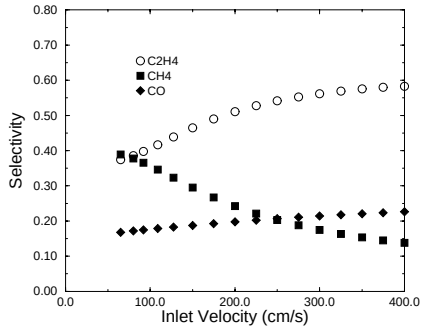

(b)

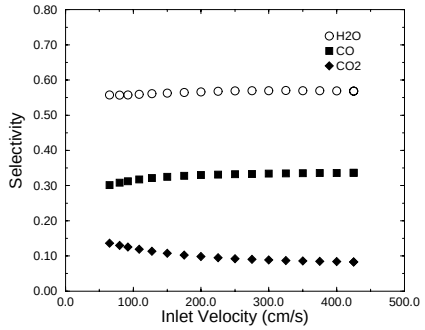

(c)

Figure 3: Conversion and selectivity as a function of inlet velocity. (a) conversion, (b) carbon selectivity, and (c) oxygen selectivity. P=1.4 atm, C/O=1.8, and T_{inlet}=300 K.

and (c) oxygen selectivity for select species. For all parameter studies to follow, the same organization of the figures for (a), (b), and (c) are used. The conversion of the carbon containing species (ethane in Figure 3a) is one of the critical parameters that must be maximized. Note that to keep the conversion of ethane near unity, the velocity can not increase above 220 cm/s. The observed effects were due to breakthrough, the flow is too fast for the reactant and intermediate species to interact with the catalytic surface. The second critical parameter is the selectivity to ethylene in Figure 3b. Note that with increasing velocity (corresponding to a drop in conversion) there is a large increase in selectivity. This points out a fundamental trade off which was found to hold true under all conditions. As the conversion was increased, the selectivity to the desired product decreased.

The next parameter to study was the carbon to oxygen ratio to see if the chemistry behaves according the experimental observations from Veser and Schmidt [14]. Figure 4 depicts the conversion and selectivities for an increasing C/O ratio from 1.8 to 2.4. Note that there is an extreme drop in conversion (down to 65%) with a marginal increase in ethylene selectivity. The C/O parameter is critical in maximizing the efficiency of this reactor system.

Figure 5 shows the standard conversion and selectivity plots for a continuation study of the reactor pressure parameter. The interesting behavior is that the selectivity goes through a maximum around 4.5 atm. The conversion drops drastically with increasing pressure so the logical pressure to operate at is 4.5 atm where the conversion has only dropped to $\sim$93%. The ethylene selectivity and conversion only vary by about 10% over the entire range of C/O ratios, making the operating pressure a secondary variable in terms of impact on ethylene production.

Figure 6 depicts the conversion and selectivity as a function of inlet temperature. The conversion increased from 90% to 100% as the temperature was increased from 300 K to 600 K. Selectivity dropped by $\sim$15%. Since the velocity was kept constant during the parameter continuation, as the inlet temperature increased, the overall inlet mass flow rate decreased. Therefore we expect Figure 6 to exhibit the opposite behavior to that of the inlet velocity study (Figure 3). The trends in selectivity in both figures are similar, but the overall values are different (shifted by about 5%), indicating that the

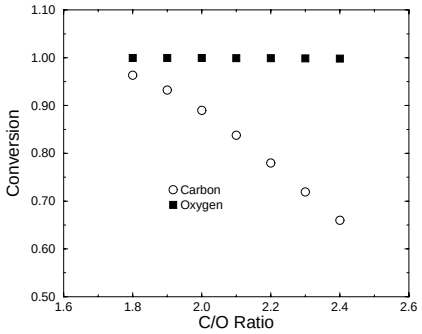

(a)

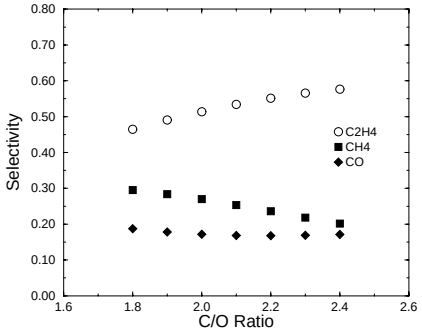

(b)

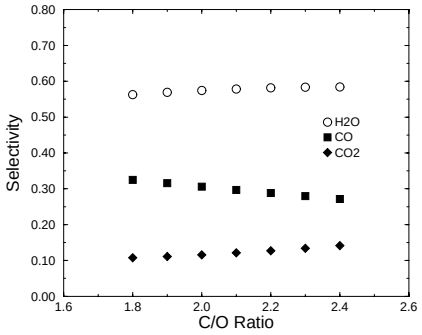

(c)

Figure 4: Conversion and selectivity as a function of carbon to oxygen ratio. (a) conversion, (b) carbon selectivity, and (c) oxygen selectivity. V_{inlet}=150 cm/s, T_{inlet}=300 K and P=1.4 atm.

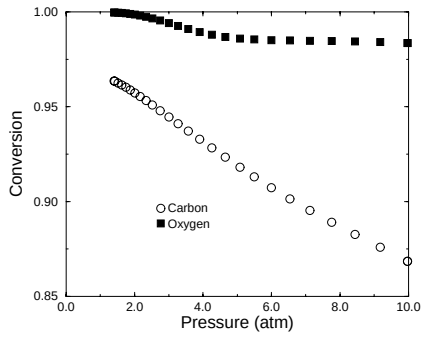

(a)

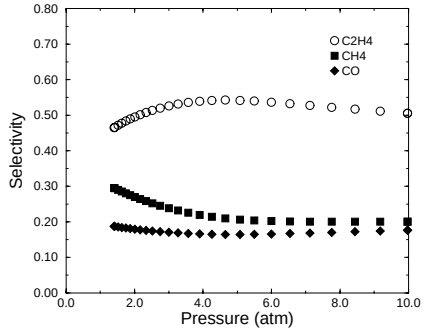

(b)

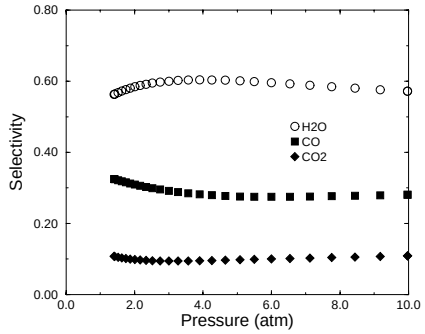

(c)

Figure 5: Conversion and selectivity as a function of reactor pressure. (a) conversion, (b) carbon selectivity, and (c) oxygen selectivity. V_{inlet}=150 cm/s, C/O=1.8, and T_{inlet}=300 K.

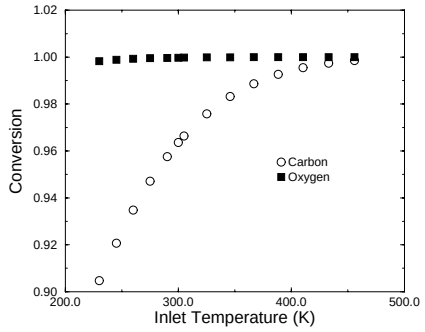

(a)

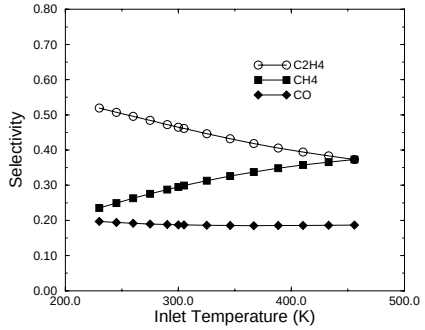

(b)

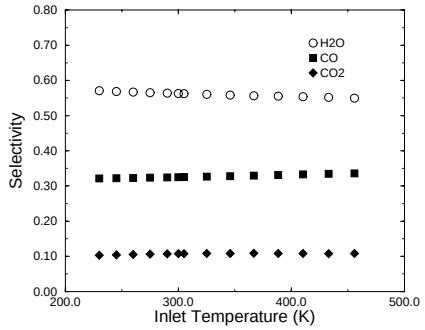

(c)

Figure 6: Conversion and selectivity as a function of inlet temperature. (a) conversion, (b) carbon selectivity, and (c) oxygen selectivity. V_{inlet}=150 cm/s, C/O=1.8, and P=1.4 atm.

inlet temperature does slightly influence the chemistry. The carbon selectivity to ethylene drops while the selectivity to methane increases. The higher temperatures favor the formation of methane over ethylene as depicted in Figure 6b. Therefore, the reactants should come in cold to reduce attacks on the ethane molecule before the surface has a chance to initiate the partial oxidation reactions.

Tube radius was the next factor analyzed. Figure 7 shows the conversion and selectivity as a function of tube radius. The wall thickness was kept constant while the inside radius was varied from 0.25 mm to 0.8 mm. The conversion drops by 45% as the radius is increased. This is the result of breakthrough. As the radius of the channel widens, there is less influence of the catalytic surface on the bulk flow. It should be pointed out that the inlet velocity was kept constant as the radius increased, and not the inlet mass flow rate. This kept the residence times roughly equal, allowing for the comparison. It is interesting that while the conversion shows a drastic drop, the selectivity to ethylene goes through a maximum. This points to the fact that the selectivity to ethylene is not controlled by either the surface chemistry, the gas-phase chemistry, or transport, but a combination of all three. Increasing the radius lessens the influence of the surface chemistry on the bulk flow. As the radius is increased from 0.25 mm to 0.58 mm, the selectivity increases. At radii greater than 0.58 mm the selectivity drops, presumable due to breakthrough because the surface chemistry has lost too much influence. This points to competition of the surface reactions with the gas-phase reactions. The bottom line is that the surface and gas-phase chemistry are highly coupled in producing ethylene, and the interplay between each must be controlled for efficient production. This harks back to the point that the reactor design of CPO systems requires even small scale studies to be run at industrial production conditions to construct a well designed system. Tube radius was found to be a critical parameter in ethylene selectivity.

It should also be noted that the catalyst length was kept constant at 1 cm. In communications with Dave Zerkle and the research group from DOW, the common consensus was that only the leading edge and the first few mm of the catalyst controlled the reaction and that catalyst length and surface area were not factors in determining conversion or selectivity. Bodke and Schmidt also came to the same conclusion [1].

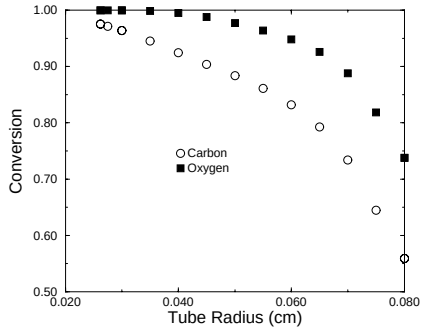

(a)

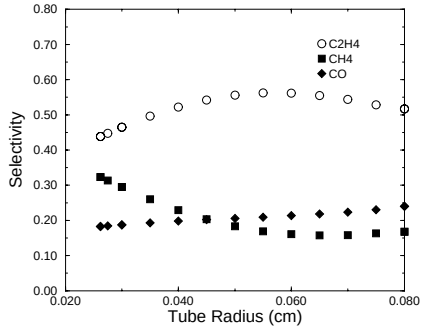

(b)

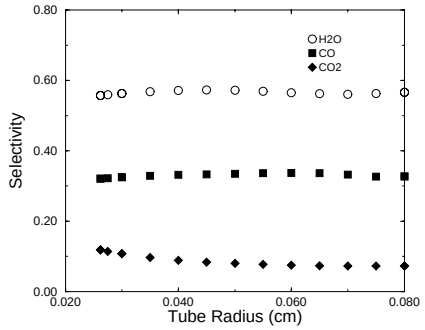

(c)

Figure 7: Conversion and selectivity as a function of tube radius. (a) conversion, (b) carbon selectivity, and (c) oxygen selectivity. V_{inlet}=150 cm/s, T_{inlet}=300 K, C/O=1.8, and P=1.4 atm.

While the maximization of both the conversion of ethane and the selectivity to ethylene are the major goals, other factor must be accounted for. The production of CO and CO_2 should be minimized since they contribute to environmental pollution. The chemistry tended to separate into various paths based on the products. The four major paths (these are *not* elementary mechanism steps) [14] are:

$$C_2H_6 + 3.5O_2 \rightleftharpoons 2CO_2 + 3H_2O \tag{1}$$

$$C_2H_6 + 2.5O_2 \rightleftharpoons 2CO + 3H_2O \tag{2}$$

$$C_2H_6 + O_2 \rightleftharpoons 2CO + 3H_2 \tag{3}$$

$$C_2H_6 + 0.5O_2 \rightleftharpoons C_2H_4 + H_2O \tag{4}$$

Equation 1 is total oxidation while equations 2 to 4 are the partial oxidation routes. Total oxidation corresponds to fuel-lean combustion conditions while the partial oxidation results typically occur under fuel-rich conditions [14]. It is evident that in the partial oxidation processes, oxygen can attack either the carbon atoms to form CO and CO_2 or attack hydrogen atoms, stripping them from ethane to form water and in the process, produce ethylene. Increasing the carbon selectivity towards ethylene and away from CO and CO_2 means that free oxygen in the gas-phase must be bound before it can attack carbon. The idea is to insert a radical scavenger into the flow that has a higher affinity to oxygen than carbon. Therefore, hydrogen was introduced into the feed. Schmidt and coworkers have found that with certain catalysts, a selectivity of >85% can be achieved [1, 4] with the addition of hydrogen. Hydrogen was inserted into the feed for a parametric study of the H/O ratio ranging from 0.0 to 2.3. Figure 8 shows how the conversion and selectivity are affected by the addition of hydrogen. The carbon conversion increases to unity as hydrogen is added. What is unexpected is that the selectivity toward ethylene decreases rapidly with increasing hydrogen concentrations. This observation points to a missing branch in the chemistry mechanism since much experimental data has been accumulated for increasing ethylene selectivity with hydrogen addition. Note also that the selectivity to CO and CO_2 drops off as hydrogen input is increased. This is expected since the oxygen is not free to attack the carbon species. Despite the shortcomings of the mechanism for hydrogen addition, the mechanism can still be used to draw some important conclusions about the CPO of ethane to ethylene. Figure 10 depicts the mass fractions for selected species for when hydrogen is

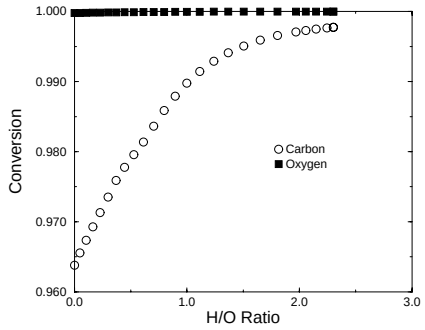

(a)

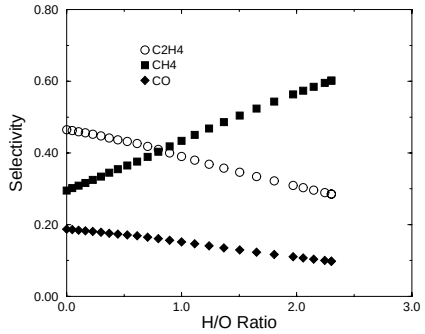

(b)

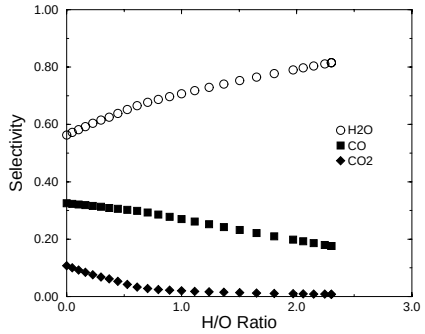

(c)

Figure 8: Conversion and selectivity as a function of hydrogen to oxygen ratio. (a) conversion, (b) carbon selectivity, and (c) oxygen selectivity. V_{inlet}=150 cm/s, T_{inlet}=300 K, C/O=1.8, and P=1.4 atm.

not present in the feed (H/O=0.0) and for when it is present (H/O=2.3). The interesting behavior is that the CO and CO_2 production drops as hydrogen is added. As commented previously, hydrogen binds with the oxygen to form water, thus preventing oxygen from attacking the carbon species. The surface sites on the catalyst are also of interest. Figure 10 depicts the surface site fractions of species as a function of position down the catalyst length. Only species with site fractions greater than 10^{-3} are plotted. Note that with the addition of hydrogen, the site fraction of surface hydrogen increases while the site fraction of surface CO drops as expected.

These preliminary results show that the selectivity to ethylene can be influenced by all of the above parameters, but do not indicate a way to reach selectivities over 60

The parametric study has elucidated the inlet velocities at which breakthrough begins, the sensitive relationship of the C/O ratio to the conversion, the reactor pressure which maximizes carbon selectivity to ethylene, the effect of tube radius on production parameters, and the effects of hydrogen addition to the inlet stream.

3.1 Backward Facing Step

Once the parametric study was accomplished, geometry studies became the focus. One geometry study has been completed and is the subject of this section. Referring back to Figure 2 note that for the CO_2 mass fraction, a high concentration (a spike) occurs near the leading edge of the catalyst. CO_2 is an unwanted byproduct because it reduces the carbon selectivity towards ethylene, and is a greenhouse gas. One idea was to change the geometry near the leading edge of the catalyst such the the boundary layer would increase. This may delay or even remove the spike in CO_2 concentration, significantly reducing CO_2 emissions. To this end, a backward facing step was added to the heat shield section (the 1 cm section before the catalyst) of the reactor. This modification meant that the tube radius for the heat shield section was smaller than that for the rest of the reactor with the transition in tube radius represented as a step change.

Figure 11 is a zoomed view of the mass fraction of CO_2 near the leading

Parameter	No Step	Backward Step
Carbon Conversion	0.9638	0.9669
Oxygen Conversion	0.9998	0.9998
Carbon Selectivity to Ethylene	0.4649	0.4606
Carbon Selectivity to CO	0.1873	0.1861
Carbon Selectivity to Methane	0.2953	0.3001
Oxygen Selectivity to H_2O	0.5628	0.5624
Oxygen Selectivity to CO	0.3251	0.3240
Oxygen Selectivity to CO_2	0.1073	0.1087

Table 2: Summary of the conversion and selectivities for selected species.

edge of the catalyst surface. The mesh lines are superimposed on the plot. The spike in CO_2 is positioned on the right edge of the first element of the catalyst surface. Since the peak is centered on one single node, this suggests the CO_2 spike may be a numerical problem associated with the transition from a no flux boundary condition (heat shield) to a flux boundary condition (catalyst surface) on the inside tube surface. While this is the most likely explanation, there is compelling evidence to the contrary. First, there is no spike in concentration for any other species at that node, and at the trailing edge of the catalyst, there is no spike at all (where there is also a flux/no flux transition). Second, when hydrogen is added, the spike disappears. The fact that chemistry can eliminate the spike makes it more likely that the spike is a real phenomena. Figure 12 is a plot of the mass fraction of CO_2 for (a) the standard conditions in the normal tube, (b) the backward step at standard conditions, and (c) the standard conditions in the normal tube with a H/O ratio of 2.3. The figure depicts the elimination of the spike with the addition of hydrogen to the feed.

It is interesting to note that the thicker boundary layer created by the backward facing step did not decrease production of CO_2, but slightly increased it. This means that the CO_2 production is surface mediated with the slight increase in the peak mass fraction coming from the desorption of CO_2 from the surface and subsequent trapping of CO_2 in the recirculation on the back edge of the step.

Table 2 compares the critical parameters (conversion and selectivity of se-

lected species) with and without the backward facing step. There is almost no difference between the two cases, meaning the step is not a design factor which affects conversion.

4 Conclusions

The sensitivity of the conversion and selectivities to various operating conditions and geometries was explored. From this parametric study, optimal design parameters and operating conditions were identified. An initial study on adding geometric shapes to the inside of the tube was also undertaken to ascertain the effects of boundary layer thickness on CO_2 production. Future work includes adding concave and convex curves to the catalyst surface and tube walls to study the effects of boundary layer thickness at lengths further down the catalyst. 3D simulations will then be utilized to ascertain how conversion and selectivity change when going from a straight tube channel to a bent or curved configuration (tortuous channels) such as would be expected in foam monoliths.

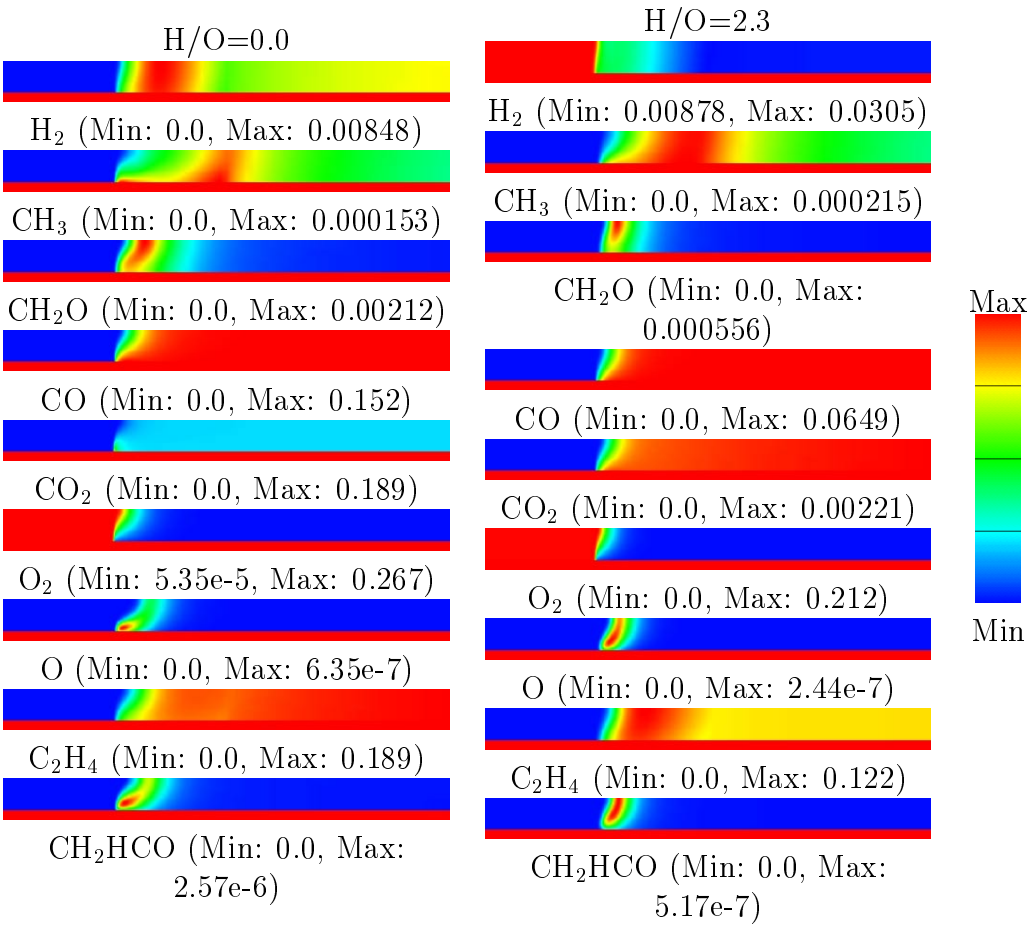

Figure 9: A comparison of the mass fraction of selected species when hydrogen is added to the feed at the standard conditions. V_{inlet}=150 cm/s, P=1.4 atm, C/O=1.8, and T_{inlet}=300 K.

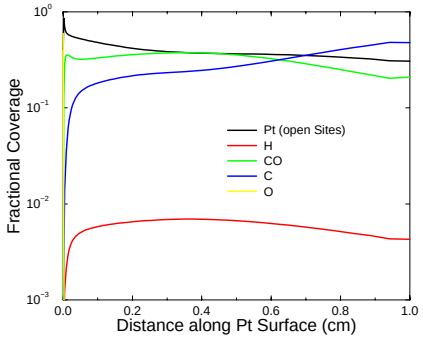

(a)

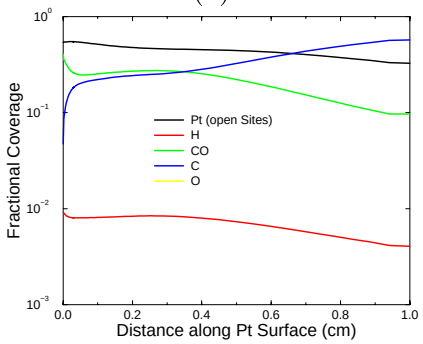

(b)

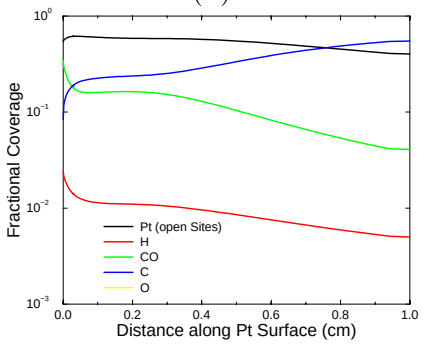

(c)

Figure 10: Surface site fractions for species with fractional coverage > 1.0e-3 for different hydrogen to oxygen ratios. (a) H/O=0.0, (b) H/O=1.0, and (c) H/O=2.3. V_{inlet}=150 cm/s, T_{inlet}=300 K, C/O=1.8, and P=1.4 atm.

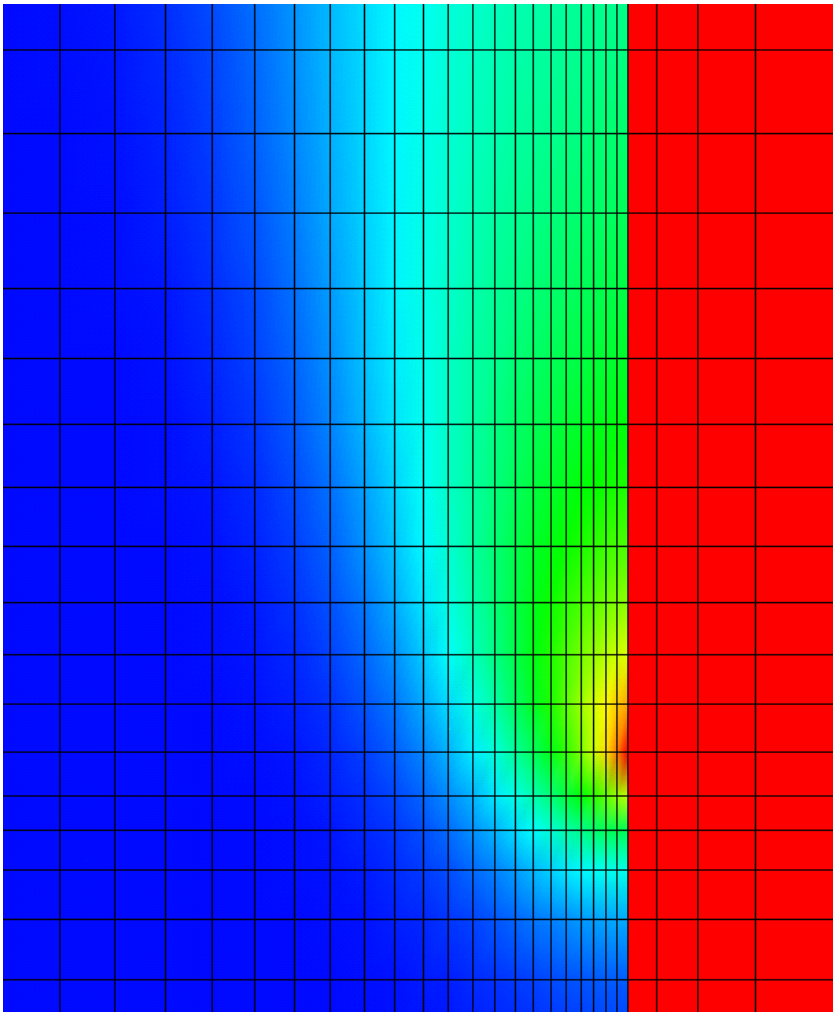

Figure 11: Zoomed view of the CO_2 mass fraction near the leading edge of the catalyst under standard conditions. V_{inlet}=150 cm/s, P=1.4 atm, C/O=1.8, H/O=0.0, and T_{inlet}=300 K.

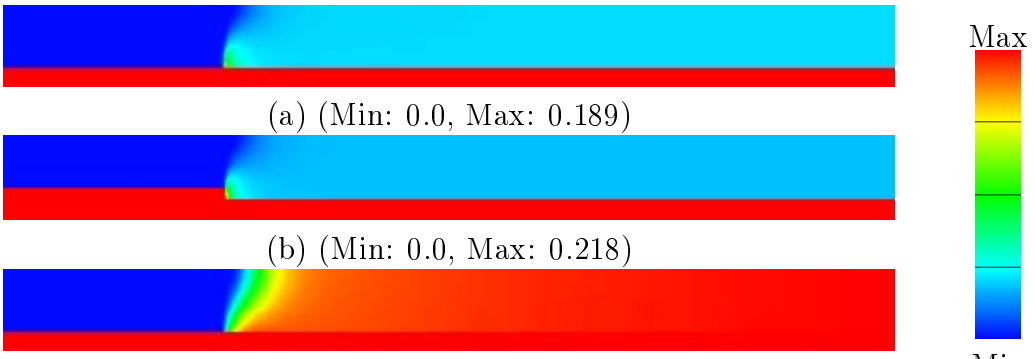

(a) (Min: 0.0, Max: 0.189)

(b) (Min: 0.0, Max: 0.218)

(c) (Min: 0.0, Max: 0.00221)

Figure 12: A comparison of the mass fraction of CO_2 selected where the geometry is modified to add a backward facing step to the leading edge of the catalyst. (a) standard tube, (b) backward facing step modification, (c) standard tube with hydrogen added to the inlet feed (H/O=2.3). V_{inlet}=150 cm/s, P=1.4 atm, C/O=1.8, H/O=0.0, and T_{inlet}=300 K.

Appendix A: Chemistry Mechanism

The following mechanisms are written in the Chemkin and Surface Chemkin format [15, 16]. The mechanism was supplied by Dave Zerkle of Los Alamos National Laboratories in collaboration with Mark Allendorf of Sandia National Laboratories.

4.1 Gas-phase Mechanism

No.	*Reaction*	Ko	β	Ea
1	$OH + H2 = H + H2O$	2.14E+08	1.52	3449.0
2	$O + OH = O2 + H$	2.02E+14	-0.4	0.0
3	$O + H2 = OH + H$	5.06E+04	2.67	6290.0
4	$H + O2(+M) = HO2(+M)$	4.52E+13	0.0	0.0
	$LOW/$	1.05E+19	-1.257	0.0 /
	$H2O/0.0/H2/0.0/CH4/10.0/CO2/3.8/CO/1.9/$			
5	$H + O2(+H2) = HO2(+H2)$	4.52E+13	0.0	0.0
	$LOW/$	1.52E+19	-1.133	0.0 /
6	$H + O2(+H2O) = HO2(+H2O)$	4.52E+13	0.0	0.0
	$LOW/$	2.10E+23	-2.437	0.0 /
7	$OH + HO2 = H2O + O2$	2.13E+28	-4.827	3500.0
	DUP			
8	$OH + HO2 = H2O + O2$	9.10E+14	0.0	10964.0
	DUP			
9	$H + HO2 = OH + OH$	1.50E+14	0.0	1000.0
10	$H + HO2 = H2 + O2$	8.45E+11	0.65	1241.0
11	$H + HO2 = O + H2O$	3.01E+13	0.0	1721.0
12	$O + HO2 = O2 + OH$	3.25E+13	0.0	0.0
13	$OH + OH = O + H2O$	3.57E+04	2.4	-2112.0
14	$H + H + M = H2 + M$	1.00E+18	-1.0	0.0
	$H2O/0.0/H2/0.0/$			
15	$H + H + H2 = H2 + H2$	9.20E+16	-0.6	0.0
16	$H + H + H2O = H2 + H2O$	6.00E+19	-1.25	0.0
17	$H + OH + M = H2O + M$	2.21E+22	-2.0	0.0
	$H2O/6.4/$			

No.	*Reaction*	Ko	β	Ea
18	$H+O+M=OH+M$	4.71E+18	-1.0	0.0
	$H2O/6.4/$			
19	$O+O+M=O2+M$	1.89E+13	0.0	-1788.0
20	$HO2+HO2=H2O2+O2$	4.20E+14	0.0	11982.0
	DUP			
21	$HO2+HO2=H2O2+O2$	1.30E+11	0.0	-1629.0
	DUP			
22	$OH+OH(+M)=H2O2(+M)$	1.24E+14	-0.37	0.0
	$LOW/$	3.04E+30	-4.63	2049.0 /
	$TROE/0.470100.02000.01.0E+15/$			
23	$H2O2+H=HO2+H2$	1.98E+06	2.0	2435.0
24	$H2O2+H=OH+H2O$	3.07E+13	0.0	4217.0
25	$H2O2+O=OH+HO2$	9.55E+06	2.0	3970.0
26	$H2O2+OH=H2O+HO2$	2.40E+00	4.042	-2162.0
27	$CH3+CH3(+M)=C2H6(+M)$	9.22E+16	-1.174	636.0
	$LOW/$	1.14E+36	-5.246	1705.0/
	$TROE/0.4051120.069.61.0E+15/$			
	$H2O/5.0/H2/2.0/CO2/3.0/CO/2.0/$			
28	$CH3+H(+M)=CH4(+M)$	2.14E+15	-0.4	0.0
	$LOW/$	3.31E+30	-4.0	2108.0 /
	$TROE/0.01.0E-151.0E-1540.0/$			
	$H2O/5.0/H2/2.0/CO2/3.0/CO/2.0/$			
29	$CH3+HO2=CH4+O2$	3.00E+12	0.0	0.0
30	$CH3+O=CH2O+H$	8.00E+13	0.0	0.0
31	$CH2O+OH=HCO+H2O$	3.43E+09	1.18	-447.0
32	$CH2O+H=HCO+H2$	2.19E+08	1.77	3000.0
33	$CH2O+O=HCO+OH$	1.80E+13	0.0	3080.0
34	$HCO+O2=HO2+CO$	7.58E+12	0.0	410.0
35	$HCO+M=H+CO+M$	1.86E+17	-1.0	17000.0
	$H2O/5.0/H2/1.87/CO2/3.0/CO/1.87/CH4/2.81/$			
36	$HCO+OH=H2O+CO$	1.00E+14	0.0	0.0
37	$HCO+H=CO+H2$	1.19E+13	0.25	0.0
38	$HCO+O=CO+OH$	3.00E+13	0.0	0.0
39	$HCO+O=CO2+H$	3.00E+13	0.0	0.0

No.	*Reaction*	Ko	β	Ea
40	$CO + OH = CO2 + H$	9.42E+03	2.25	-2351.0
41	$CO + O + M = CO2 + M$	6.17E+14	0.0	3000.0
42	$CO + O2 = CO2 + O$	2.53E+12	0.0	47688.0
43	$CO + HO2 = CO2 + OH$	5.80E+13	0.0	22934.0
44	$C2H6 + CH3 = C2H5 + CH4$	5.50E-01	4.0	8300.0
45	$C2H6 + H = C2H5 + H2$	5.40E+02	3.5	5210.0
46	$C2H6 + O = C2H5 + OH$	3.00E+07	2.0	5115.0
47	$C2H6 + OH = C2H5 + H2O$	7.23E+06	2.0	864.0
48	$C2H5 + H = C2H4 + H2$	1.25E+14	0.0	8000.0
49	$C2H5 + H = CH3 + CH3$	3.00E+13	0.0	0.0
50	$C2H5 + H = C2H6$	7.00E+13	0.0	0.0
51	$C2H5 + OH = C2H4 + H2O$	4.00E+13	0.0	0.0
52	$C2H5 + HO2 = CH3 + CH2O + OH$	3.00E+13	0.0	0.0
53	$C2H5 + O2 = C2H4 + HO2$	3.00E+20	-2.86	6760.0
	DUP			
54	$C2H5 + O2 = C2H4 + HO2$	2.12E-6	6.0	9484.0
	DUP			
55	$C2H4 + H = C2H3 + H2$	3.36E-07	6.0	1692.0
56	$C2H4 + OH = C2H3 + H2O$	2.02E+13	0.0	5936.0
57	$C2H4 + O = CH2HCO + H$	3.39E+06	1.88	179.0
58	$C2H4 + CH3 = C2H3 + CH4$	6.62E+00	3.7	9500.0
59	$C2H4 + H(+M) = C2H5(+M)$	1.08E+12	0.454	1822.0
	$LOW/$	1.112E+34	-5.0	4448.0 /
	$TROE/1.01.0E-1595.0200.0/$			
	$H2O/5.0/H2/2.0/CO2/3.0/CO/2.0/$			
60	$C2H3 + H(+M) = C2H4(+M)$	6.1E12	0.27	280.
	$LOW/$	9.8E29	-3.86	3320./
	$TROE/0.782208.2663.6095./$			
	$H2O/5.0/$			
61	$C2H3 + H = C2H2 + H2$	4.00E+13	0.0	0.0
62	$C2H3 + O = CH2CO + H$	3.00E+13	0.0	0.0
63	$C2H3 + O2 = CH2O + HCO$	1.7E29	-5.312	6500.
64	$C2H3 + O2 = CH2HCO + O$	3.5E14	-0.611	5260.
65	$C2H3 + O2 = C2H2 + HO2$	2.12E-06	6.0	9484.0

No.	*Reaction*	Ko	β	Ea
66	$C2H3 + OH = C2H2 + H2O$	2.00E+13	0.0	0.0
67	$C2H3 + CH3 = C2H2 + CH4$	2.00E+13	0.0	0.0
68	$C2H3 + C2H3 = C2H4 + C2H2$	1.45E+13	0.0	0.0
69	$C2H2 + OH = CH2CO + H$	2.18E-04	4.5	-1000.0
	DUP			
70	$C2H2 + OH = CH2CO + H$	2.00E+11	0.0	0.0
	DUP			
71	$CH2HCO + H = CH2CO + H2$	4.00E+13	0.0	0.0
72	$CH2HCO + O = CH2O + HCO$	1.00E+14	0.0	0.0
73	$CH2HCO + OH = CH2CO + H2O$	3.00E+13	0.0	0.0
74	$CH2HCO + O2 = CH2O + CO + OH$	3.00E+10	0.0	0.0
75	$CH2HCO + CH3 => C2H5 + CO + H$	4.90E+14	-0.50	0.0
76	$CH2HCO = CH2CO + H$	3.95E+38	-7.649	45115.0
77	$CH2CO + H = CH3 + CO$	7.00E+12	0.0	3011.0

4.2 Surface Mechanism

No.	*Reaction*	Ko	β	Ea
	Adsorption			
1	$H2 + PT(s) + PT(s) => H(s) + H(s)$	0.046E-00	0.0	0.0
	$STICKCOV/PT(s)$	0.0	-1.0	0.0/
2	$O2 + PT(s) + PT(s) => O(s) + O(s)$	1.345E+22	-0.5	0.0
3	$CH4 + PT(s) + PT(s) <=> CH3(s) + H(s)$	6.000E-01	0.0	72.20
	$STICK$			
4	$H2O + PT(s) <=> H2O(s)$	1.000E-01	0.0	0.0
	$STICK$			
5	$CO2 + PT(s) <=> CO2(s)$	5.000E-03	0.0	0.00
	$STICK$			
6	$CO + PT(s) => CO(s)$	8.400E-01	0.0	0.0
	$STICK$			
7	$C2H6 + PT(s) + PT(s) => C2H5(s) + H(s)$	3.000E-01	0.0	50.0
	$STICK$			
8	$C2H4 + PT(s) => C2H4(1s)$	1.000E-03	0.0	0.0
	$STICK$			
	Desorption			
9	$H(s) + H(s) => PT(s) + PT(s) + H2$	3.700E+21	0.0	72.8
	$COV/H(s)$	0.0	0.0	-6.0/
10	$O(s) + O(s) => PT(s) + PT(s) + O2$	3.700E+21	0.0	213.0
	$COV/O(s)$	0.0	0.0	-60.0/
11	$CO(s) => CO + PT(s)$	1.000E+13	0.0	145.9
12	$C2H5(s) + H(s) => PT(s) + PT(s) + C2H6$	3.700E+21	0.0	130.0
13	$C2H4(1s) => PT(s) + C2H4$	1.000E+13	0.0	130.0
	Surface Reactions			
14	$O(s) + H(s) <=> OH(s) + PT(s)$	3.700E+21	0.0	11.5
15	$H(s) + OH(s) <=> H2O(s) + PT(s)$	3.700E+21	0.0	17.4
16	$OH(s) + OH(s) <=> H2O(s) + O(s)$	3.700E+21	0.0	48.2
17	$CO(s) + O(s) => CO2(s) + PT(s)$	3.700E+21	0.0	105.0
18	$CO2(s) + PT(s) => CO(s) + O(s)$	3.700E+20	0.0	162.9
19	$C(s) + O(s) <=> CO(s) + PT(s)$	3.700E+21	0.0	62.8
20	$CH3(s) + PT(s) <=> CH2(s) + H(s)$	1.262E+22	0.0	70.3
21	$CH2(s) + PT(s) <=> CH(s) + H(s)$	7.000E+22	0.0	59.0

No.	*Reaction*	Ko	β	Ea
22	$CH(s) + PT(s) <=> C(s) + H(s)$	3.000E+22	0.0	00.0
23	$C2H4(1s) => C2H4(2s)$	1.000E+13	0.0	83.3
24	$C2H4(2s) => C2H4(1s)$	1.000E+13	0.0	75.3
25	$CH2(s) + CH3(s) => C2H5(s) + PT(s)$	3.700E+21	0.0	00.0
26	$C2H5(s) + PT(s) => CH2(s) + CH3(s)$	3.700E+21	0.0	128.9
27	$C2H5(s) + PT(s) => C2H4(2s) + H(s)$	3.700E+21	0.0	54.4
28	$C2H4(2s) + H(s) => C2H5(s) + PT(s)$	3.700E+21	0.0	29.3
29	$C2H4(2s) + PT(s) => CH3(s) + CH(s)$	3.700E+21	0.0	182.8
30	$CH3(s) + CH(s) => C2H4(2s) + PT(s)$	3.700E+21	0.0	0.0
31	$C2H4(2s) + PT(s) => C2H3(1s) + H(s)$	3.700E+21	0.0	99.1
32	$C2H3(1s) + H(s) => C2H4(2s) + PT(s)$	3.700E+21	0.0	75.3
34	$C2H3(1s) + PT(s) => CH3(s) + C(s)$	3.700E+21	0.0	46.0
35	$CH3(s) + C(s) => C2H3(1s) + PT(s)$	3.700E+21	0.0	46.9

Acknowledgements

The authors would like to thank the following people for helping guide this work: Jon Siddall and Tyler Thompson at The Dow Chemical Company, Lanny Schmidt at the University of Minnesota, David Zerkle of Los Alamos National Lab, and Steve Rice, Nancy Jackson, Mark Allendorf, and John Shadid at Sandia National Labs. This work was supported by DOE's Office of Industrial Technologies Industries of the Future program, building on work funded by the DOE Mathematical, Informational, and Computational Sciences Division. Sandia is a multiprogram laboratory operated by Sandia Corporation, a Lockheed-Martin Company, for the United States Department of Energy under Contract DE-AC04-94AL85000.

References

[1] A. S. Bodke, D. A. Olschki, L. D. Schmidt, and E. Ranzi. High selectivities to ethylene by partial oxidation of ethane. *Science*, 258:712–715, 1999.

[2] M. Huff and L. D. Schmidt. Ethylene formation by oxidative dehydrogenation of ethane over monoliths at very short contact times. *Journal of Physical Chemistry*, 97:11815, 1993.

[3] M. Huff and L. D. Schmidt. Elementary step model of ethane oxidative dehydrogenation on pt-coated monoliths. *AIChE Journal*, 42(12):3484–3497, 1996.

[4] A. S. Bodke and L. D. Schmidt. Oxidative dehydrogenation of ethane at millisecond contact times: Effects of h_2 addition. manuscript in preparation, August 1999.

[5] L. D. Schmidt, M. Huff, and S. S. Bharadwaj. Catalytic partial oxidation reactions and reactors. *Chemical Engineering Science*, 49(24A):3981–3994, 1994.

[6] D. A. Hickman and L. D. Schmidt. Modeling catalytic gauze reactors: Ammonia oxidation. *Industrial & Engineering Chemistry Research*, 30:50, 1991.

[7] C. N. Satterfield. *Heterogeneous Catalysis in Industrial Practice*. McGraw-Hill, New York, 1991.

[8] C. T. Goralski Jr., L. D. Schmidt, and W. L. Brown. Catalytic incineration of VOC containing air streams at very short contact times. *AIChE Journal*, 1998.

[9] O. Deutschmann and L. D. Schmidt. Partial oxidation of methane in a short contact time reactor: Two-dimensional modeling with detailed chemistry. *submitted to AIChE Journal*, 1998.

[10] D. A. Hickman and L. D. Schmidt. Production of syngas by direct catalytic oxidation of methane. *Science*, 259:343–346, 1993.

[11] D. A. Hickman and L. D. Schmidt. Synthesis gas formation by direct oxidation of methane over Pt monoliths. *Journal of Catalysis*, 138:267–282, 1992.

[12] D. A. Hickman, E. A. Haupfear, and L. D. Schmidt. Syngas formation by direct oxidation of methane over Rh monoliths. *Catalysis Letters*, 17:223, 1993.

[13] D. A. Hickman and L. D. Schmidt. Synthesis gas formation by direct oxidation of methane over monoliths. In *Catal. Select. Oxid.*, volume 32 of *ACS Proc.*, pages 416–426, 1993.

[14] G. Veser and L. D. Schmidt. Ignition and extinction in the catalytic oxidation of hydrocarbons over platinum. *AIChE Journal*, 42(4):1077–1087, 1996.

[15] R. Kee, F. M. Rupley, E. Meeks, and J. A. Miller. Chemkin-III: A fortran chemical kinetics package for the analysis of gas-phase chemical and plasma kinetics. Technical report, Sandia National Laboratories, Albuquerque, New Mexico 87185, 1996. SAND96-8216.

[16] M. E. Coltrin, R. Kee, F. M. Rupley, and E. Meeks. Surface Chemkin-III: A fortran package for analyzing heterogeneous chemical kinetics at a solid-surface—gas-phase interface. Technical report, Sandia National Laboratories, Albuquerque, New Mexico 87185, 1996. SAND96-8217.